Towards topological analysis of non-symmetric tensor fields via complexification

Bernhard Burgeth[1][0000−0001−6602−6201], Andreas Kleefeld*[2,3][0000−0001−8324−821X], Eugene Zhang[4][0000−0003−4752−3119], and Yue Zhang[5][0000−0002−8467−2781]

[1] Saarland University, Faculty of Mathematics and Computer Science, 66041 Saarbrücken, Germany
burgeth@math.uni-sb.de
[2] Forschungszentrum Jülich GmbH, Jülich Supercomputing Centre, Wilhelm-Johnen-Straße, 52425 Jülich, Germany
a.kleefeld@fz-juelich.de
[3] University of Applied Sciences Aachen, Faculty of Medical Engineering and Technomathematics, Heinrich-Mußmann-Str. 1, 52428 Jülich, Germany
[4] Oregon State University, School of Electrical Engineering and Computer Science, Corvallis, OR 97331, USA
zhange@engr.orst.edu
[5] Oregon State University, School of Electrical Engineering and Computer Science, Corvallis, OR 97331, USA
zhangyue@oregonstate.edu

Abstract. Fields of asymmetric tensors play an important role in many applications such as medical imaging (diffusion tensor magnetic resonance imaging), physics, and civil engineering (for example Cauchy-Green-deformation tensor, strain tensor with local rotations, etc.). However, such asymmetric tensors are usually symmetrized and then further processed. Using this procedure results in a loss of information. A new method for the processing of asymmetric tensor fields is proposed restricting our attention to tensors of second-order given by a 2×2 array or matrix with real entries. This is achieved by a transformation resulting in Hermitian matrices that have an eigendecomposition similar to symmetric matrices. With this new idea numerical results for real-world data arising from a deformation of an object by external forces are given. It is shown that the asymmetric part indeed contains valuable information.

Keywords: asymmetric tensor fields · spectral decomposition · line integral convolution.

1 Introduction

Fields of tensors are an essential notion in many applications such as medical imaging, physics, and civil engineering. Tensors make their natural appearance

* Corresponding author

as Cauchy-Green-deformation tensor, strain tensor with local rotations, permittivity tensor, etc., or as structure tensor in image processing itself. Although the notion of a tensor is quite sophisticated especially in mathematical literature, in the context of this article we consider them simply as 2×2-arrays of complex numbers subjected to the standard computational rules of matrix calculus. Despite this fact, we refer to any mapping from a suitable set $\Omega \subset \mathbb{R}^2$ into the set of matrices as a tensor field as it is common.

Symmetric matrices or second order tensors possess an eigenvalue decomposition with real eigenvalues and mutually orthogonal eigenvectors. Hence, a decomposition of a symmetric matrix S as

$$S = Q \cdot D \cdot Q^\top$$

with a diagonal matrix D and an orthogonal matrix Q is at our disposal. As a consequence the functional calculus is sufficiently rich to pave the way to transfer algorithms designed for the processing of real-valued data (functions) to the setting of matrix-valued data (functions), let us refer to [4].

The visualization of symmetric tensors often makes use of the corresponding quadratic form resulting in ellipses ($n = 2$) or ellipsoids ($n = 3$) (see for example [8]), casting the information about eigenvalues and eigenvectors in an appealing visual form. Particular visualization methodologies focus on the overall appearance of the tensor field, its topological, global structure, and its connectivity. Prominent is the line integral convolution (LIC) procedure that relies on the dominant eigenvector, that is the (normalized) eigenvector belonging to the largest eigenvalue of a symmetric matrix [5]. Clearly this concepts is no longer applicable if the existence of a real-valued eigenvector cannot be guaranteed as it is the case for general non-symmetric, hence, mostly non-diagonalizable matrices. However, tensors of the latter type are of particular interest in many applications. As a remedy a symmetrization is used leading to a manageable tensor field, but at the price of a loss of the information captured in the asymmetric part.

This is the reason why existing research [1, 7, 9–11] even in the 2D-case is based on their visualization of asymmetric tensor fields relying on the decomposition of an asymmetric tensor into the product of three matrix components, whose corresponding physical concepts in civil engineering are respectively expansion/contraction, rotation, and pure shear. But these approaches have their intricacies and their generalization to dimension $n = 3$ does not seem to be straightforward.

In this article, our response to this dilemma is "complexifying" the asymmetric tensors by applying a mapping Ξ from the set of real square matrices $\mathbb{R}^{n\times n}$ into the set of Hermitian tensors $\mathrm{Herm}(n) := \{K \in \mathbb{C}^{n\times n} : K = K^*\}$ with $n \geq 2$ defined by (see also [2, 3])

$$\Xi : \begin{cases} \mathbb{R}^{n\times n} & \longrightarrow \quad \mathrm{Herm}(n) \\ A & \longmapsto \frac{1}{2}(A + A^\top) + \frac{\mathrm{i}}{2}(A - A^\top)\,. \end{cases} \tag{1}$$

We will elaborate more on this mapping Ξ in Section 2, while we report on the application of hermitization together with the LIC-procedure to real data sets in Section 3. A short summary and an outlook is given in Section 4.

2 The conversion process

Since tensors describing general deformation fields are usually not symmetric, they are symmetrized leading to a loss of information captured in the asymmetric part. In this article, those tensors are pre-processed by applying a mapping Ξ given by (1) in the special case $n = 2$. Indeed, for any $A \in \mathbb{R}^{2\times 2}$ we have $(\Xi(A))^* = \Xi(A)$, where $^\top$ and * means transpose and conjugate transpose, respectively. The reason for this pre-processing step is the fact that Hermitian tensors allow for a rich tensor (or matrix) calculus almost as amenable as in the case of real symmetric matrices since in both cases the matrices form a real vector space and are unitarily diagonalizable with real eigenvalues. We point out that some properties of this mapping and Hermitian tensors also hold for $n \geq 2$.

Proposition 1. *Ξ maps $\mathbb{R}^{n\times n}$ bijectivly into the real vector space* $\mathrm{Herm}(n)$.

Proof. The mapping Ξ is linear on a finite dimensional space and has a trivial kernel. Hence, it is an isomorphism and therefore invertible.

For the sake of brevity we set $H = (H_{ij})_{i,j=1,2} := \Xi(T)$ and assume

$$H = U\Lambda U^*\,, \qquad \Lambda = \mathrm{diag}(\kappa_1, \kappa_2)$$

with real eigenvalues $\kappa_1 \geq \kappa_2$. A straightforward reckoning reveals

$$\kappa_1 = (H_{11} + H_{22})/2 + \sqrt{(H_{11} + H_{22})^2/4 - (H_{11}H_{22} - H_{12}H_{21})} \tag{2}$$

and for the associated major eigenvector (not normalized)

$$u_1 = (H_{12}, -(H_{11} - \kappa_1))^\top .$$

The second component of u_1 is real, that is, $\mathrm{Im}(-(H_{11} - \kappa_1)) = 0$. That means the imaginary part of this major eigenvector is aligned in the real x-direction.

Remark 1. Note that the eigenvector u_1 can be multiplied by an arbitrary constant, say $c \in \mathbb{C}$, and still it will be an eigenvector. In fact, we can specifically choose $c = \mathrm{e}^{\mathrm{i}\beta}$ with $\beta \in [0, 2\pi]$ without changing the original length of the eigenvector. That means we could theoretically align the major eigenvector in any direction (if desired).

3 Numerical results

Note that all the following figures are created with Matlab 2018a. The line integral convolution algorithm has been downloaded from the web page

https://itp.tugraz.at/~ahi/Uni/AppSoft/LIC/

which has been implemented in Matlab by A. Hirczy.

Further, note that the data are generated from two real experiments. Precisely, the 2D tensor fields we are dealing with in this section are derived from the deformation of an object by external forces. The strain tensor is derived from the gradient of the displacement occurring when external forces to an object are applied (see [6, Section 2.2.3]). Here, we consider two configurations of forces, indicated by the arrows in Fig. 1, acting on a 2D object of a square-like shape with coordinates $[-0.675, 0.675] \times [-0.675, 0.675]$. Non-zero forces are acting on the right side of the square-shaped body, resembling a parabolic force pattern in the first case (data set named "*parabolic*"), while the pattern is more sinusoidal in the second case (data set named "*sinusoidal*").

First, we will visualize the non-symmetric stress tensor field obtained from the deformation gradient. Precisely, taking the partial derivative of the displacement vector field with respect to the material coordinates gives the material displacement gradient tensor which can be written as $F - I$ where F is the deformation gradient tensor field (see [6, Section 2.1.6 and Section 2.2.3]).

The stress tensor under consideration is a multiplication between a symmetric stress tensor and the deformation gradient tensor. It is an asymmetric tensor, thus it might give us some new insight.

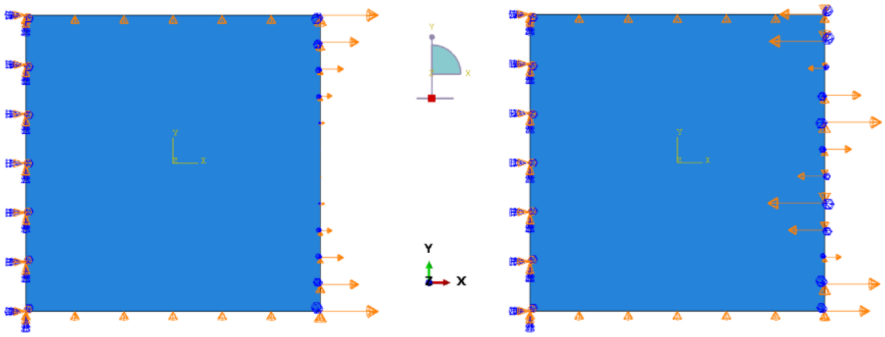

Fig. 1. The two experiments *parabolic* and *sinusoidal*.

3.1 Non-symmetric stress tensor

Each of the resulting data sets are stress tensor fields with a (pixel) resolution of 217×217. We transform the non-symmetric matrix into a Hermitian matrix for each pixel and compute the real and imaginary part of the major eigenvector corresponding to κ_1 of (2). In sum, this results in two different vector fields. From these vector fields integral lines are derived through convolution and visualized

by the LIC procedure. In addition, we plot the major eigenvector fields in quiver plots as an alternative representation method for better visual comparison. Note that we only visualize every fifth vector resulting in a 43×43 resolution to avoid cluttering. We begin with the *parabolic* data set.

When the imaginary part is aligned in positive x-direction, then we color the arrow in green. Otherwise, it is colored red, as shown in Fig. 2. Both the LIC-

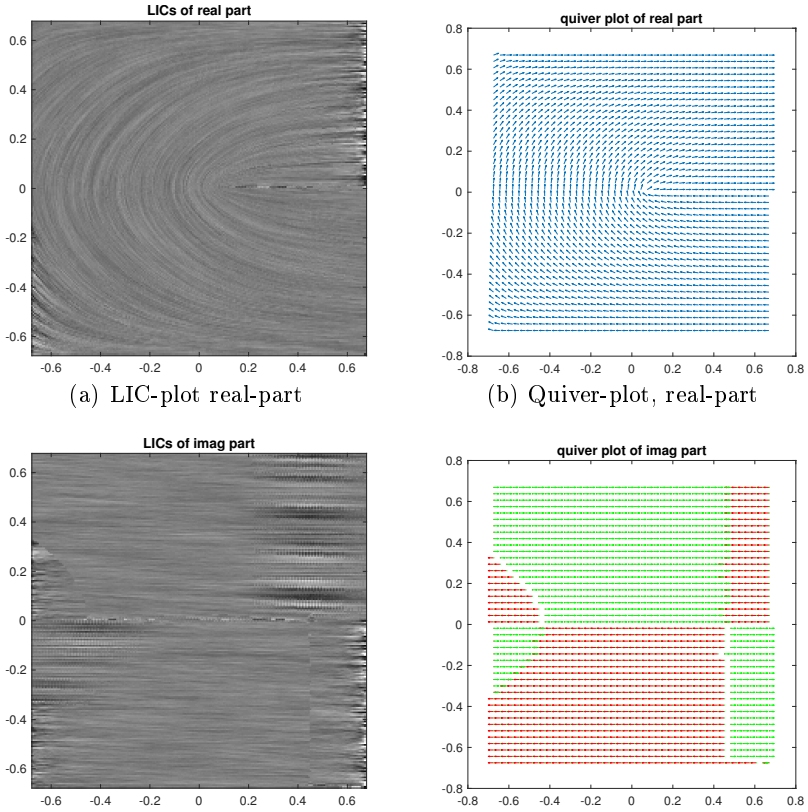

(a) LIC-plot real-part (b) Quiver-plot, real-part

(c) LIC-plot, imaginary-part (d) Quiver-plot, imaginary-part

Fig. 2. First column: Graphical representation of the line integral convolution (LIC) of the real and imaginary part of the eigenvector corresponding to κ_1 of (2) for the data set *parabolic* having resolution 217×217. Second column: Thinned out quiver plots (43×43 resolution) of the real and imaginary part of the same eigenvector fields.

representation and the quiver plot of the real part of the major eigenvector field clearly indicates that the *parabolic* pattern of forces applied on the right hand side of the shape creates a corresponding response inside. The anti-symmetric "left-right" pattern in the imaginary part of the major eigenvector field is a striking feature in the quiver-plot while it is not so clearly discernible in the LIC-picture.

The later is no surprise since by its very construction the LIC-procedure is not predisposed to capture the discontinuous behavior of the imaginary part of the vector components.

In some applications, where tensorial quantities are derived from gradients, for example, indefinite matrices may play a role. Using polar decomposition for symmetrization inevitably causes positive definiteness of the resulting tensor, which means an additional loss of information. Nevertheless, even in the case of positivity, the asymmetry captured in the imaginary part of the Hermitian tensor reveals discontinuity properties of the data (visible in the quiver plots) that are independent of the rotational ambiguity mentioned in Remark 1, and hence they should not be discarded. Whether these discontinuities indicate possible locations of emerging fractures in materials or real anomalies in flow patterns is not yet clear. At this stage of our research a reasonable and authoritative explanation still eludes the authors.

For the sake of comparison, we show in Fig. 3 the major eigenvector field in its LIC-representation after the non-symmetric stress tensor data have been symmetrized in each pixel simply by means of $A \mapsto (A + A^\top)/2$.

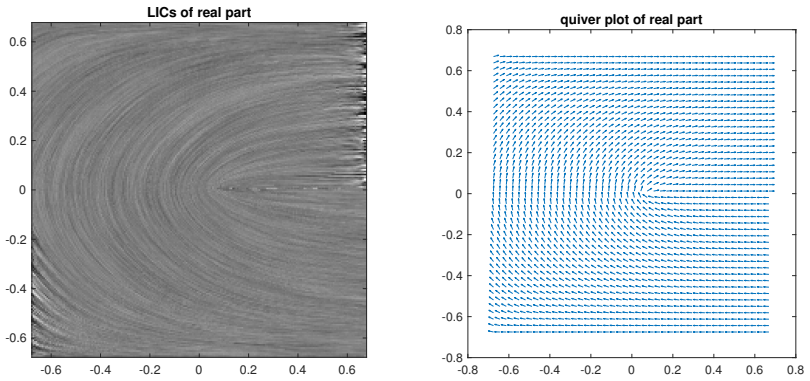

(a) LIC-plot, symmetrized data (b) Quiver-plot, symmetrized data

Fig. 3. Left: Graphical representation of the line integral convolution (LIC) of the eigenvector corresponding to κ_1 of the symmetrization $(A + A^\top)/2$ for the data set *parabolic*. Right: Thinned out quiver plots (43×43 resolution) of the same symmetrized real eigenvector fields.

As expected, the imaginary part is zero and does not contain any information, hence we refrain from a graphical representation. A comparison of the major eigenvector field stemming from the real part of the hermitization versus the symmetrized tensor field reveals very little differences in the LIC-representation as well as in the quiver plot. The reason might be that the non-symmetry in the original data is not very pronounced and hence the imaginary part is rather small. Nevertheless, the similarity between hermitization and symmetrized version speaks for the reliability of the proposed approach.

Next, we process and visualize the stress tensor fields stemming from the *sinusoidal* data set as illustrated in Fig. 4.

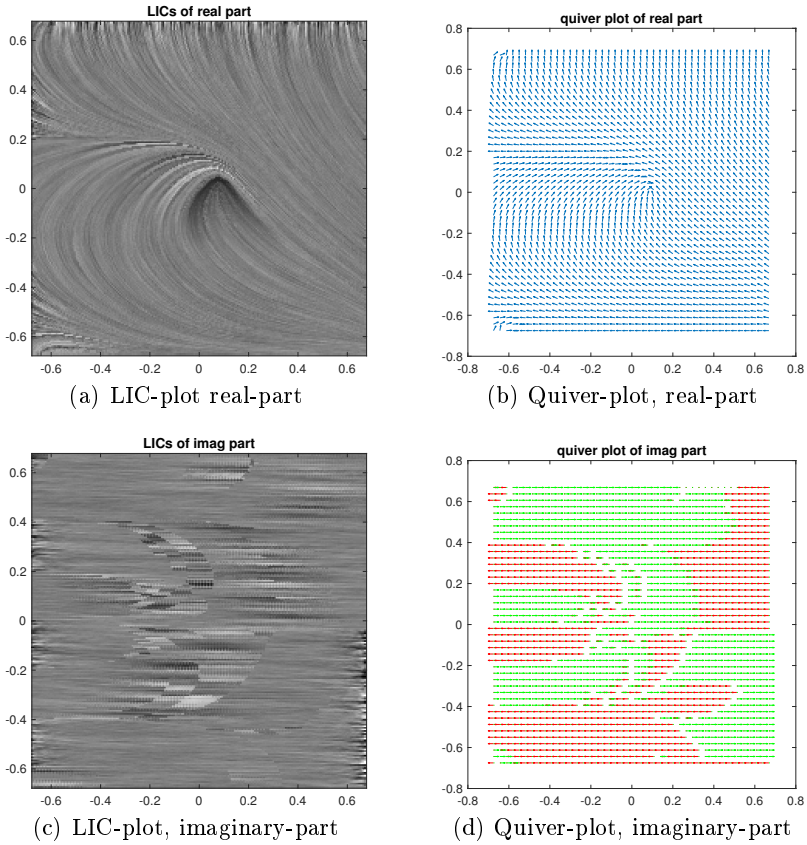

(a) LIC-plot real-part (b) Quiver-plot, real-part

(c) LIC-plot, imaginary-part (d) Quiver-plot, imaginary-part

Fig. 4. First column: Graphical representation of the line integral convolution (LIC) of the real and imaginary part of the eigenvector corresponding to κ_1 of (2) for the data set *sinusoidal* having resolution 217×217. Second column: Thinned out quiver plots (43×43 resolution) of the real and imaginary part of the same eigenvector fields.

The LIC-representation and the quiver plot of the real part of the major eigenvector field reveal an eddy-like structure inside the shape as a response to the *sinusoidal* pattern of forces applied on the right border. The LIC image of the imaginary part of the major eigenvector field indicates a complicated pattern inside the object, and as before, the quiver plot capable of capturing the discontinuous "left-right" pattern, provides a similar but more discernible internal structure. A thorough interpretation of such newly discovered pattern will be the subject of future research.

For comparison, we show in Fig. 5 the major eigenvector after applying line integral convolution to data being symmetrized via $(A + A^\top)/2$ in each pixel.

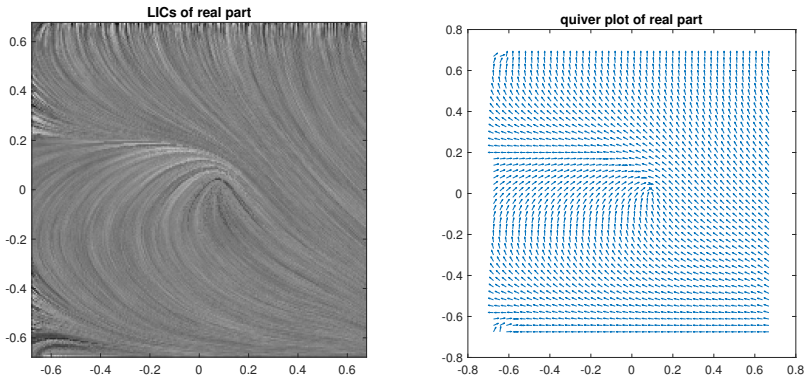

(a) LIC-plot, symmetrized data (b) Quiver-plot, symmetrized data

Fig. 5. Left: Graphical representation of the line integral convolution (LIC) of the eigenvector corresponding to κ_1 of the symmetrization $(A + A^\top)/2$ for the data set *sinusoidal*. Right: Thinned out quiver plots (43×43 resolution) of the same symmetrized real eigenvector fields.

Again, the vanishing imaginary part is not graphically represented. In contrast to the findings for the previous data set a comparison of the major eigenvector field stemming from the real part of the hermitization versus the symmetrized tensor field reveals significant differences in the LIC-representation as well as in the quiver plot. We attribute this to a more pronounced non-symmetry and a larger imaginary component if compared with the first data set. The data set *sinusoidal* suggests that symmetrization indeed destroys a significant portion of information and that this information not only might be preserved by hermitization but also, via its imaginary part, might eventually lead to new interpretations and insights.

3.2 Deformation gradient tensor

The deformation gradient tensor as a non-symmetric tensor is a meaningful quantity, but it is not very much studied in the literature. We proceed almost as before. We extract the deformation gradient tensor fields for both force configurations (*parabolic* and *sinusoidal*), we use hermitization and then produce graphical LIC and quiver representations as shown in Figs. 6 and 7.

In case of the data set *parabolic* the LIC representations of the deformation gradient tensor field and the stress tensor field (refer to Fig. 2) look very much the same if we look at the real part of the major eigenvector fields. Seemingly, the same holds true for the quiver plots. However, the imaginary part exhibits

some differences between the deformation gradient field and the stress tensor field both in the LIC and the quiver plot, albeit more pronounced in the latter one, as expected.

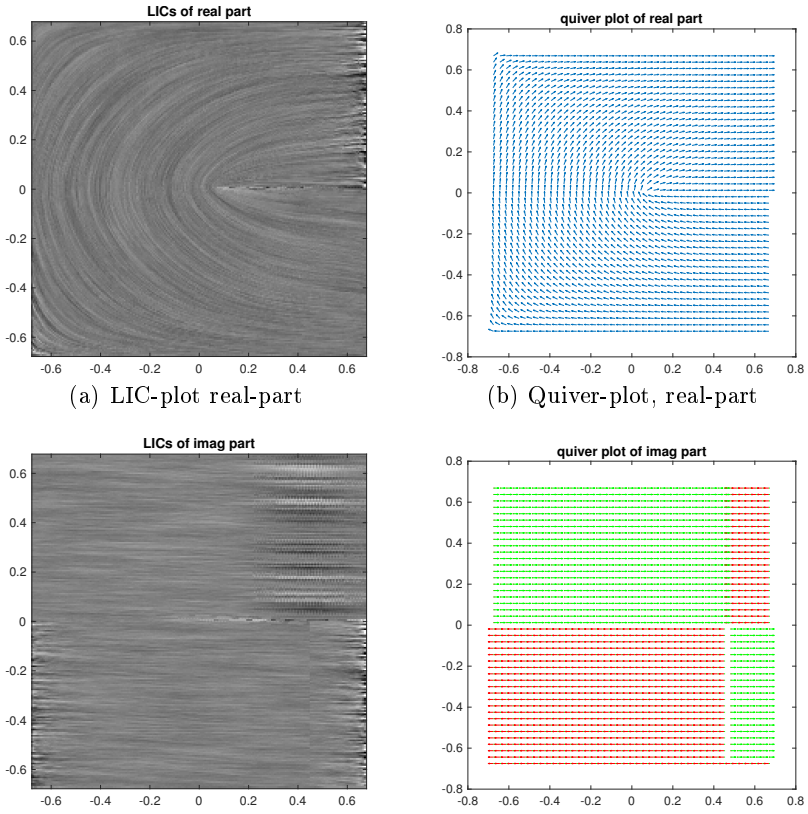

(a) LIC-plot real-part (b) Quiver-plot, real-part

(c) LIC-plot, imaginary-part (d) Quiver-plot, imaginary-part

Fig. 6. First column: Graphical representation of the line integral convolution (LIC) of the real and imaginary part of the eigenvector corresponding to κ_1 of (2) for the data set *parabolic* having resolution 217×217. Second column: Thinned out quiver plots (43×43 resolution) of the real and imaginary part of the same eigenvector fields.

The situation is different for the *sinusoidal* data set. We note some discrepancies between the deformation gradient field, see Fig. 7, and the corresponding stress tensor field, see Fig. 4, in all four representations, namely, LIC- and quiver plots, real and imaginary parts.

The experiments show, that significant information about a field of non-symmetric tensors is captured in the imaginary parts of its hermitization form, which solely results from the non-symmetry. The outcome suggests that symmetrization of the tensors indeed eliminates information to some extent. The

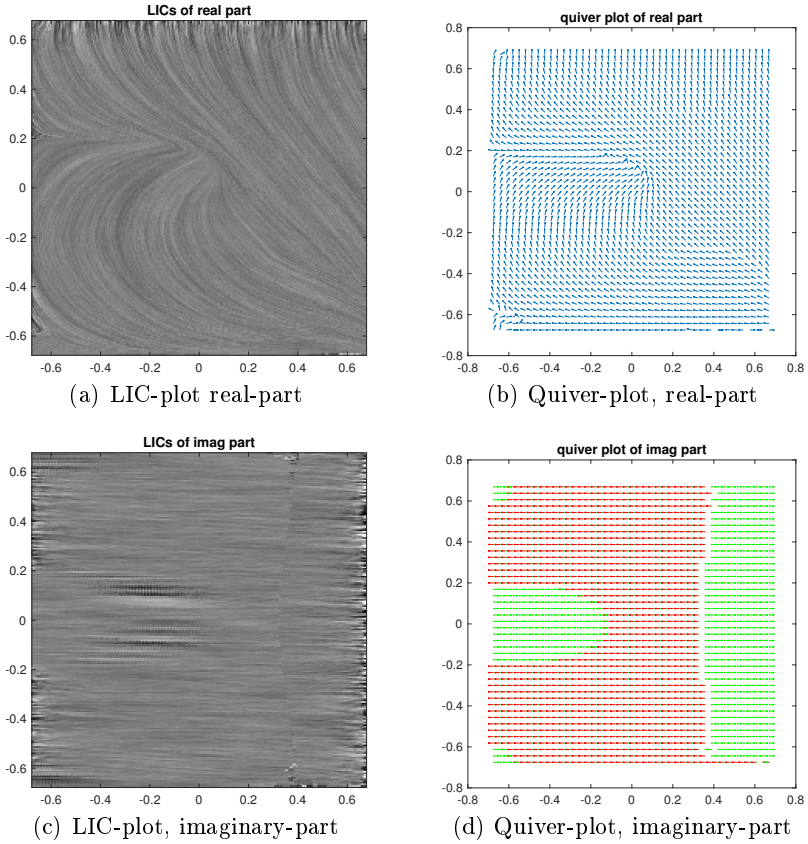

(a) LIC-plot real-part (b) Quiver-plot, real-part

(c) LIC-plot, imaginary-part (d) Quiver-plot, imaginary-part

Fig. 7. First column: Graphical representation of the line integral convolution (LIC) of the real and imaginary part of the eigenvector corresponding to κ_1 of (2) for the data set *sinusoidal* having resolution 217×217. Second column: Thinned out quiver plots (43×43 resolution) of the real and imaginary part of the same eigenvector fields.

imaginary part of the major eigenvector field displayed in quiver plots reveals this information, however, those plots by no means lend themselves to a straightforward interpretation; hence more research is needed in this direction.

4 Summary and outlook

There are numerous examples of real second-order tensors in medical imaging or civil engineering that are symmetric, hence they have an eigendecomposition, which allows for a rather straightforward processing and analysis. However, the original tensors encountered in applications might not be symmetric. Their analysis and processing is much more cumbersome, since SVD and Jordan decomposition are complicated and sometimes insufficient substitutes for the lack of

an eigendecomposition. In order to circumvent this difficulty, the tensors are often symmetrized, and the asymmetric part is discarded, but this possibly comes with the price of loosing the information captured in the asymmetry. Rewriting a non-symmetric tensor as a Hermitian tensor, hermitization for short, allows to preserve this information since Hermitian matrices possess an eigendecomposition as well. However, the eigenvectors have complex-valued components, which means, that the non-symmetry information is mainly cast into the imaginary part of the eigenvectors while its real part is very close to the one stemming from the symmetrized version. Although the complex eigenvector may be shifted in phase (i.e. multiplied by $e^{i\beta}$ with $\beta \in [0, 2\pi]$) the abrupt discontinuous behavior of the imaginary part of the major eigenvector identifies edges in the tensor field that clearly stem from the asymmetric parts of the tensors.

The numerical results on non-symmetric 2D stress and deformation gradient tensor fields clearly indicate that this part of information is indeed relevant, albeit difficult to interpret from the quiver and LIC-plots.

In fact, we hope to find a better connection of the presented subject to image processing and mathematical morphology in the future. The discovered discontinuity represents a boundary of a region. If the external force pattern changes, then this region will change as well leading to a moving boundary. Maybe this movement can be related to some morphological operation. Knowledge of this connection might enable us to predict the boundary of a yet unknown force field. Hence, the extensive simulation of the mechanical response of external forces applied to materials can be replaced by simple morphological operations to obtain the location of such a discontinuity. This is especially relevant in three dimensions.

More tests and research efforts in this direction will be a topic of our future research.

References

1. Auer, C., Kasten, J., Kratz, A., Zhang, E., Hotz, I.: Automatic, tensor-guided illustrative vector field visualization. In: 2013 IEEE Pacific Visualization Symposium. pp. 265–272. IEEE, Sydney (2013). https://doi.org/10.1109/PacificVis.2013.6596154
2. Burgeth, B., Kleefeld, A.: Towards processing fields of general real-valued square matrices. In: Schultz, T., Özarslan, E., Hotz, I. (eds.) Modeling, Analysis, and Visualization of Anisotropy. pp. 115–144. Mathematics and Visualization, Springer, Cham (2017). https://doi.org/10.1007/978-3-319-61358-1_6
3. Burgeth, B., Kleefeld, A.: A unified approach to PDE-driven morphology for fields of orthogonal and generalized doubly-stochastic matrices. In: Angulo, J., Velasco-Forero, S., Meyer, F. (eds.) Mathematical Morphology and Its Applications to Signal and Image Processing. LNCS, vol. 10225, pp. 284–295. Springer, Cham (2017). https://doi.org/10.1007/978-3-319-57240-6_23
4. Burgeth, B., Pizarro, L., Breuß, M., Weickert, J.: Adaptive continuous-scale morphology for matrix fields. International Journal of Computer Vision **92**(2), 146–161 (2011). https://doi.org/10.1007/s11263-009-0311-4

5. Cabral, B., Leedom, L.C.: Imaging vector fields using line integral convolution. In: Proceedings of the 20th Annual Conference on Computer Graphics and Interactive Techniques. pp. 263–270. SIGGRAPH '93, ACM, New York (1993). https://doi.org/10.1145/166117.166151
6. Dimitrienko, Y.I.: Nonlinear Continuum Mechanics and Large Inelastic Deformations, Solid Mechanics and Its Applications, vol. 174. Springer, New York (2011). https://doi.org/10.1007/978-94-007-0034-5
7. Khan, F., Roy, L., Zhang, E., Qu, B., Hung, S.H., Yeh, H., Laramee, R.S., Zhang, Y.: Multi-scale topological analysis of asymmetric tensor fields on surfaces. IEEE Transactions on Visualization and Computer Graphics **26**(1), 270–279 (2020). https://doi.org/10.1109/TVCG.2019.2934314
8. O'Meara, O.: Introduction to Quadratic Forms. Classics in Mathematics, Springer, Berlin (2000). https://doi.org/10.1007/978-3-642-62031-7
9. Palke, D., Lin, Z., Chen, G., Yeh, H., Vincent, P., Laramee, R.S., Zhang, E.: Asymmetric tensor field visualization for surfaces. IEEE Transactions on Visualization and Computer Graphics **17**(12), 1979–1988 (2011). https://doi.org/10.1109/TVCG.2011.170
10. Zhang, E., Yeh, H., Lin, Z., Laramee, R.S.: Asymmetric tensor analysis for flow visualization. IEEE Transactions on Visualization and Computer Graphics **15**(1), 106–122 (2009). https://doi.org/10.1109/TVCG.2008.68
11. Zheng, X., Pang, A.T.: 2D asymmetric tensor analysis. In: VIS 05. IEEE Visualization, 2005. pp. 3–10 (2005). https://doi.org/10.1109/VISUAL.2005.1532770